

LA-UR-22-22287

Accepted Manuscript

Revealing charge carrier dynamics and transport in Te-doped GaAsSb and GaAsSbN nanowires by correlating ultrafast terahertz spectroscopy and optoelectronic characterization

Yuan, Long
Pokharel, Rabin
Devkota, Shisir
Hirandeeep, Kuchoor
Lee, Min Chul (Min-Cheol)
Huang, Yue
Yarotski, Dmitry Anatolievitch
Iyer, Shanthi
Prasankumar, Rohit Prativadi

Provided by the author(s) and the Los Alamos National Laboratory (2022-08-12).

To be published in: Nanotechnology

DOI to publisher's version: 10.1088/1361-6528/ac7d61

Permalink to record:

<http://permalink.lanl.gov/object/view?what=info:lanl-repo/lareport/LA-UR-22-22287>



Los Alamos National Laboratory, an affirmative action/equal opportunity employer, is operated by Triad National Security, LLC for the National Nuclear Security Administration of U.S. Department of Energy under contract 89233218CNA000001. By approving this article, the publisher recognizes that the U.S. Government retains nonexclusive, royalty-free license to publish or reproduce the published form of this contribution, or to allow others to do so, for U.S. Government purposes. Los Alamos National Laboratory requests that the publisher identify this article as work performed under the auspices of the U.S. Department of Energy. Los Alamos National Laboratory strongly supports academic freedom and a researcher's right to publish; as an institution, however, the Laboratory does not endorse the viewpoint of a publication or guarantee its technical correctness.

Revealing Charge Carrier Dynamics and Transport in Te-Doped GaAsSb and GaAsSbN Nanowires by Correlating Ultrafast Terahertz Spectroscopy and Optoelectronic Characterization

Long Yuan^{1#}, Rabin Pokharel^{2#}, Shisir Devkota², Hirandeep Kuchoor², Kendall Dawkins², Min-Cheol Lee¹, Yue Huang¹, Dmitry A. Yarotski¹, Shanthi Iyer^{*2}, and Rohit P. Prasankumar^{*1}

Affiliations:

¹Center for Integrated Nanotechnologies, Los Alamos National Laboratory, Los Alamos, New Mexico 87545, United States

²Nanoengineering Department, Joint School of Nanoscience and Nanoengineering, North Carolina A&T University, Greensboro, North Carolina 27401, United States

Email: rpprasan@alum.mit.edu and iyer@ncat.edu

Abstract

Recent advances in the growth of III-V semiconductor nanowires (NWs) hold great promise for nanoscale optoelectronic device applications. It is established that a small amount of nitrogen (N) incorporation in III-V semiconductor NWs can effectively red-shift their wavelength of operation and tailor their electronic properties for specific applications. However, understanding the impact of N incorporation on non-equilibrium charge carrier dynamics and transport in semiconducting NWs is critical in achieving efficient semiconducting NW devices. In this work, ultrafast optical pump-terahertz probe spectroscopy has been used to study non-equilibrium carrier dynamics and transport in Te-doped GaAsSb and dilute nitride GaAsSbN NWs, with the goal of correlating these results with electrical characterization of their equilibrium photo-response under bias and low-frequency noise characteristics. Nitrogen incorporation in GaAsSb NWs led to a significant increase in the carrier scattering rate, resulting in a severe reduction in carrier mobility. Carrier recombination lifetimes of 33 ± 1 picoseconds (ps) and 147 ± 3 ps in GaAsSbN and GaAsSb NWs, respectively, were measured. The reduction in the carrier lifetime and photoinduced optical conductivities are due to the presence of N-induced defects, leading to deterioration in the electrical and optical characteristics of dilute nitride NWs relative to the non-nitride NWs. Finally, we observed a very fast rise time of ~ 2 ps for both NW materials, directly impacting their potential use as high-speed photodetectors.

1. Introduction

III-V semiconductor nanowires (NWs) have attracted significant attention for photodetection applications such as telecommunications [1, 2], biochemical sensing [3], and focal plane arrays [4] because of their low dimension and high surface-to-volume ratio, tunable bandgap, strong optical absorption [5], photonic waveguiding properties [6], and excellent carrier mobility [7]. However, due to their large surface-to-volume ratio, NWs are sensitive to surface traps, and their small cross-section also makes them vulnerable to interface traps. Furthermore, any inherent defects within the NW impact device performance. Hence, understanding carrier dynamics and transport in these nanostructures is essential for optoelectronics, especially in tailoring the carrier lifetime and mobility for a specific application.

Among III-V materials, GaAsSb has drawn particular interest due to its direct bandgap and wavelength range encompassing the near-infrared (NIR), from 850 nm to 1700 nm, which is widely used in both fiber optical communications [8, 9] and photonic integrated high-speed applications [10]. However, beyond 1300 nm, the GaAsSb NW quality and morphology deteriorate, impacting the optical properties [7]. A small amount of nitrogen (N) incorporation in the GaAsSb lattice expands the wavelength to the desired telecom range due to the huge bandgap reduction, thereby making it possible to overcome the challenges of higher Sb incorporation [11]. Another advantage lies in enhancing the electron effective mass upon N-incorporation, leading to increased electron confinement and reduced spill-out of carriers to the barriers [12, 13]. Hence, an investigation of the effect of N-incorporation on optical properties would aid in unraveling the potential of dilute nitride alloys for improving the material properties of III-V alloys. This offers a promising pathway for tailoring optoelectronic properties via defect engineering in this material system.

Dilute N incorporation in III-V semiconductor thin films has been the subject of extensive study [14-20], though such studies in NWs have been comparatively limited [21-26], and to the best of our knowledge, no ultrafast optical or terahertz (THz) studies have been done on dilute nitride NWs. One of the deleterious effects of N incorporation in the host material is the simultaneous incorporation of N-induced defects [18, 27]. Our previous studies [28-32] indicate that the defects in GaAsSb and GaAsSbN

(N-incorporated GaAsSb) can be effectively compensated by doping the NWs with Te, which provides better control over the photoconductivity and carrier mobility. Significant improvement in NW quality, as assessed by photoluminescence spectroscopy, Raman spectroscopy, and performance of photodetector devices [7, 25, 26, 33, 34], was demonstrated. However, these steady-state optical and electrical measurements provide little information on non-equilibrium charge carrier dynamics in NWs, crucial to device performance. This can be studied using ultrafast optical-pump THz probe (OPTP) spectroscopy with sub-picosecond temporal resolution, a widely used non-contact tool for directly probing carrier dynamics in semiconducting NWs [35-46]. In this work, OPTP has been used to examine Te-doped GaAsSb and Te-doped GaAsSbN NWs to provide better insight into the role of N-induced defects in charge carrier recombination and transport and correlate this with their photodetector performance. This shows the potential of this technique for assessing the impact of defects in dilute nitride NWs for future defect engineering targeted towards specific device applications.

2. Materials and methods

2.1 Sample preparation

The Te-doped GaAs_{1-x}Sb_x ($x \sim 7\%$) and dilute nitride GaAs_{1-x-y}Sb_xN_y ($x < 7\%$, $y \sim 1\%$) NWs discussed in this study were grown epitaxially on single side polished p-type <111> oriented silicon (Si) substrates using the vapor-liquid-solid (VLS) mechanism. Molecular beam epitaxy (MBE) is the enabling technology for the growth of these NWs. NW doping was carried out using a GaTe captive source at a temperature of 540⁰ C for optimum optoelectronic performance. Both NW samples were grown at a beam equivalent pressure (BEP) ratio of approximately 20, which typically yielded a GaAs thin film growth rate of 0.5 monolayers/second (ML/s). The dilute nitride samples were grown with a radio frequency (RF) N-plasma source at 300 W RF power, resulting in less than 1% nitrogen incorporation based on our earlier work on GaAsSbN material system [47]. The NWs were then passivated in-situ with Ga_{0.9}Al_{0.1}As followed by a GaAs shell at 465⁰ C in ultra-high vacuum (UHV). The detailed growth recipe for the Te-doped GaAsSb

and GaAsSbN NWs discussed here can be found elsewhere [29, 30]. The as-grown NWs were then horizontally dispersed on an AlN substrate using ultrasonic sonication for ultrafast THz measurements.

2.2 Scanning electron microscopy

As-grown Te-doped GaAsSb and GaAsSbN NWs, on p-type Si<111> substrates, were imaged using a Carl Zeiss Auriga-BU FIB field emission scanning electron microscope (SEM) as shown in Fig. 1. These NWs exhibited average lengths of $1.4\pm 0.15\ \mu\text{m}$ and $1.7\pm 0.08\ \mu\text{m}$ for non-nitride and dilute nitride samples, respectively, with corresponding average diameters of $152\pm 5\ \text{nm}$ and $215\pm 15\ \text{nm}$. The distribution of NW length and diameters for the samples under study can be found in section S1 of the supplementary information.

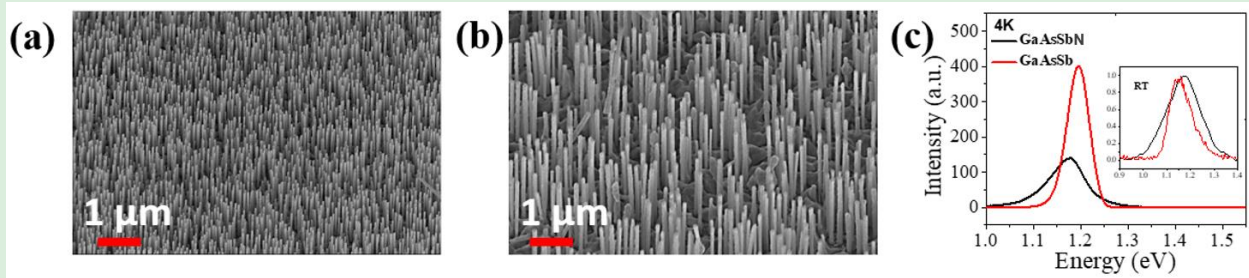


Figure 1. SEM images of ensemble Te-doped (a) GaAsSb and (b) GaAsSbN NWs. (c) Superimposed PL spectra of GaAsSb and GaAsSbN NWs at 4 K and the inset at 290 K.

2.3 Micro-photoluminescence spectroscopy

The photoluminescence spectra of NWs at both 290 K and 4 K were obtained using a home-built micro-photoluminescence (μ -PL) setup comprised of a 633 nm He-Ne laser as an excitation source, a 0.32 m double grating monochromator for wavelength dispersion, and a liquid nitrogen cooled InGaAs detector.

2.4 Electrical characterization

For NW device fabrication, the as-grown NWs on a Si <111> substrate were first spin-coated with PMMA (polymethyl methacrylate), followed by oxygen plasma etching to expose the NW tips and chemical etching to remove the NW passivation layer. Finally, Ni/Au and Ti/Au thin films were deposited onto a bare silicon substrate and exposed NW tip surfaces, respectively. Current-voltage (I-V) measurements of GaAsSb and GaAsSbN NWs were carried out using two-probe radiation shield-equipped Lake Shore TTPX probe station

integrated with a Keithley-4200 semiconductor parameter analyzer system. A micro-HR (LSH-T250) Horiba spectrometer incorporating a tungsten-halogen lamp was used for illuminating the NW device. The low-frequency noise (LFN) spectroscopy measurements, based on cross-correlation at a reverse bias of 1V, were carried out using two independent low noise current preamplifiers (SRS 570 from Stanford Research Systems) and a fast Fourier transform using a Keysight 35670A digital signal analyzer (DSA).

2.5 Ultrafast optical pump-THz probe spectroscopy

Optical pump-THz probe measurements were carried out using a home-built ultrafast THz spectrometer, as schematically shown in Fig. 2a. Briefly, a 1 kHz Ti:sapphire amplifier system was used to generate laser pulses with ~3 mJ energy, ~40 femtosecond (fs) duration, and a center photon energy of 1.55 eV. The laser output is split into three beams, where ~90% of the output power is used for THz generation by optical rectification using a ZnTe crystal. The THz beam is focused tightly onto the sample using a parabolic mirror. The transmitted THz beam through the sample is measured with electro-optic sampling in a ZnTe crystal, where the gate pulse comes from a small portion of the amplifier output. The optical pump is focused onto the sample close to normal incidence. The pump-induced changes in the transmitted THz electric field were measured at the peak of the THz waveform. The measurements were carried out in a dry nitrogen box at 290 K.

To extract the photoinduced change in the optical conductivity ($\Delta(\omega,t)$), we measured terahertz waveforms with and without photoexcitation at different time delays, allowing us to obtain the photoinduced change in the THz electric field ($\Delta E(\omega,t)/E(\omega,t)$) from Fourier transforming the corresponding THz transmission waveforms ($\Delta T(\omega,t)/T(\omega,t)$). $\Delta\sigma(\omega,t)$ is then obtained using the thin film approximation [48].

$$\Delta\sigma(\omega,t) = -\frac{\epsilon_0 c}{T} (1 + n_{sub}) \frac{\Delta E(\omega,t)}{E(\omega,t)}$$

where ϵ_0 is the permittivity of free space, c is the light speed in vacuum, T is the thickness of NWs, and n_{sub} is the refractive index of the substrate at THz frequencies.

3. Results and Discussion

Figures 1 (a) and (b) show SEM images of the as-grown Te-doped GaAsSb and GaAsSbN NWs with typical densities of $\sim 6 \times 10^8/\text{cm}^2$ and $\sim 2 \times 10^8/\text{cm}^2$, respectively, on a Si substrate (dispersed NW images not shown here). The incorporation of nitrogen atoms has a negligible effect on the size and morphology of the NWs. Figure 1(c) displays PL spectra of GaAsSb and GaAsSbN NWs at 4 K. The GaAsSbN PL spectra exhibit an asymmetric line shape, with the PL peak red-shifted by ~ 50 meV compared to the symmetric PL spectra from GaAsSb NWs. Further, the PL intensity of GaAsSbN NWs is reduced by \sim four-fold, and the spectra are correspondingly broadened (Fig. 1(c) inset) compared to the GaAsSb NWs at both 290 K and 4 K. These results provide clear spectroscopic signatures of N-induced defects at the band edges, causing potential fluctuations and widening the localized energy distribution range, as commonly reported in thin films [18].

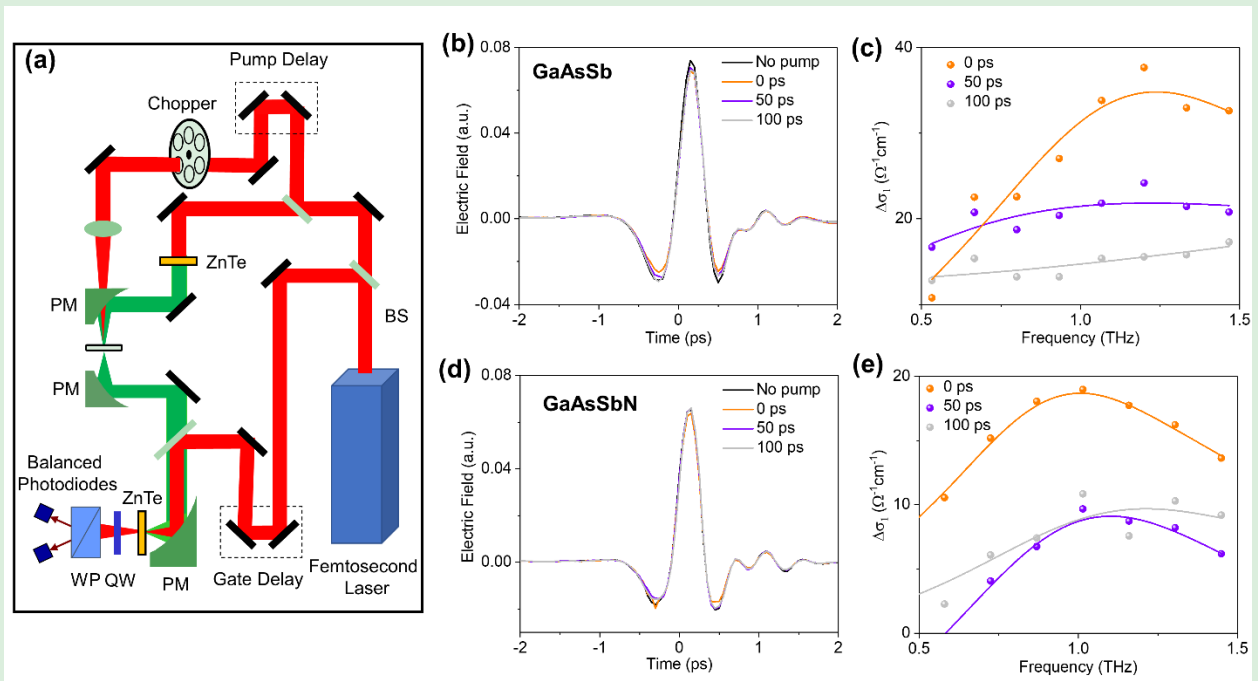


Figure 2. Transient THz conductivity measurements on GaAsSb NWs. (a) Schematic of the OPTP experiment. (BS: beam splitter; PM: parabolic mirror; QW: quarter-wave plate; WP: Wollaston prism). (b) and (d), Terahertz waveforms transmitted through GaAsSb and GaAsSbN NW at different delay times after photoexcitation with a fluence of ~ 60

$\mu\text{J}/\text{cm}^2$. (c) and (e), Photoinduced optical conductivities (real part) at different delay times. The solid lines are fits using the Drude-Lorentz oscillator model described in the main text.

Next, the dynamic transport properties of GaAsSb NWs were measured by ultrafast OPTP spectroscopy, schematically shown in Figure 2(a). Briefly, an optical pump beam with a photon energy of 1.55 eV and fluence of $\sim 60 \mu\text{J}/\text{cm}^2$ was used to excite the GaAsSb NWs. The polarization of both pump and probe beams was parallel to the sample plane. The optical pump beam (diameter ~ 4 mm) was spatially overlapped with the THz probe beam (diameter ~ 2 mm). The pump-induced change in the transmitted THz waveform ($\Delta T(\omega, t)/T(\omega, t)$) was recorded at fixed time delays between the optical pump and THz probe beams (Figures 2(b) and 2(d)). **The diameter and length of the NWs are much smaller than the THz probe wavelength, allowing us to use a thin film approximation [48] to extract the transient conductivity after photoexcitation.** The pump-induced change in the conductivity ($\Delta\sigma(\omega, t)$) was then obtained from $\Delta T(\omega, t)/T(\omega, t)$, as described above in Methods.

Figures 2(c) and (e) show the real part of $\Delta\sigma(\omega, t)$, reflecting the resistivity changes in GaAsSb and GaAsSbN NWs, respectively, induced by the pump pulses. The real part of $\Delta\sigma(\omega, t)$ is maximum at a time $t=0$ and decreases at longer time delays, proving that photoexcited carriers enhance the conductivity in semiconducting NWs. Notably, a resonance peak is observed at ~ 1 THz and attributed to localized surface plasmons (LSPs). The emergence of LSPs after photoexcitation was also observed in previous studies on GaAs and Si NWs using ultrafast THz spectroscopy [10, 35, 48]. The complex conductivity $\sigma(\omega)$ of a free electron plasma with a LSP resonance can be described using the following Drude-Lorentz oscillator model [49]:

$$\sigma(\omega) = \frac{iNe^2\omega}{m_e^*(\omega^2 - \omega_p^2 + i\omega\gamma)} \quad (1)$$

where ω_p is the LSP frequency, N is the photoexcited carrier density, m_e^* is the effective electron mass ($m_e^* = 0.063m_e$ from bulk GaAs) and γ is the momentum scattering rate. Here, two contributions, from

the bulk free electron response at $\omega_p = 0$ and the surface plasmon mode at ω_p , are considered when modeling the measured $\Delta\sigma(\omega)$. Excellent fits to $\Delta\sigma(\omega)$ using Eq. (1) are obtained at different delay times, as shown in Figures 2(c) and 2(e). The fitted parameters are listed in Table 1. The bulk carrier scattering rate in the GaAsSbN NWs is one order of magnitude higher than the non-nitride GaAsSb NWs, indicative of a pronounced nitrogen-induced effect on the carrier transport. Using the extracted momentum scattering rate, we obtained the carrier mobility:

$$\mu = \frac{e}{m_e^* \gamma} \quad (2)$$

The extracted mobilities for both samples are shown in Table 1. The bulk carrier mobility in GaAsSbN NWs is $1.48 \times 10^3 \text{ cm}^2\text{V}^{-1}\text{s}^{-1}$, which is one order of magnitude lower than in GaAsSb NWs ($1.64 \times 10^4 \text{ cm}^2\text{V}^{-1}\text{s}^{-1}$), likely due to the enhanced carrier scattering rate in the nitride alloy. These results agree well with a previous optical study showing a severe reduction in the electron mobility in n- (or p-) doped GaAs NWs [50], where the incorporation of dopants is significantly less than the N incorporation in our alloy system [30]. Another observation is the carrier scattering rate and mobility for the LSP mode are very similar in both NW samples, indicating that N incorporation primarily occurs in the bulk of the NWs. However, one has to be careful in comparing the mobilities extracted from NWs grown by different groups reported in the literature [51] as this depends on several parameters, including NW diameter, surface traps, bulk defects and the measurement techniques used.

	$N_{carrier}$ (cm^{-3})	ω_p (THz)	γ_{bulk} (s^{-1})	μ_{bulk} ($\text{cm}^2\text{V}^{-1}\text{s}^{-1}$)	$\gamma_{surface}$ (s^{-1})	$\mu_{surface}$ ($\text{cm}^2\text{V}^{-1}\text{s}^{-1}$)
GaAsSb	1.1×10^{15}	1.49	1.64×10^{12}	1.64×10^4	1.24×10^{12}	2.25×10^4
GaAsSbN	5.1×10^{14}	1.00	1.89×10^{13}	1.48×10^3	1.00×10^{12}	2.79×10^4

Table 1. Fitting parameters ($N_{carrier}$, ω_p , γ_{bulk} , $\gamma_{surface}$) using Equation 1 and extracted carrier mobility (μ_{bulk} , $\mu_{surface}$) from Equation 2.

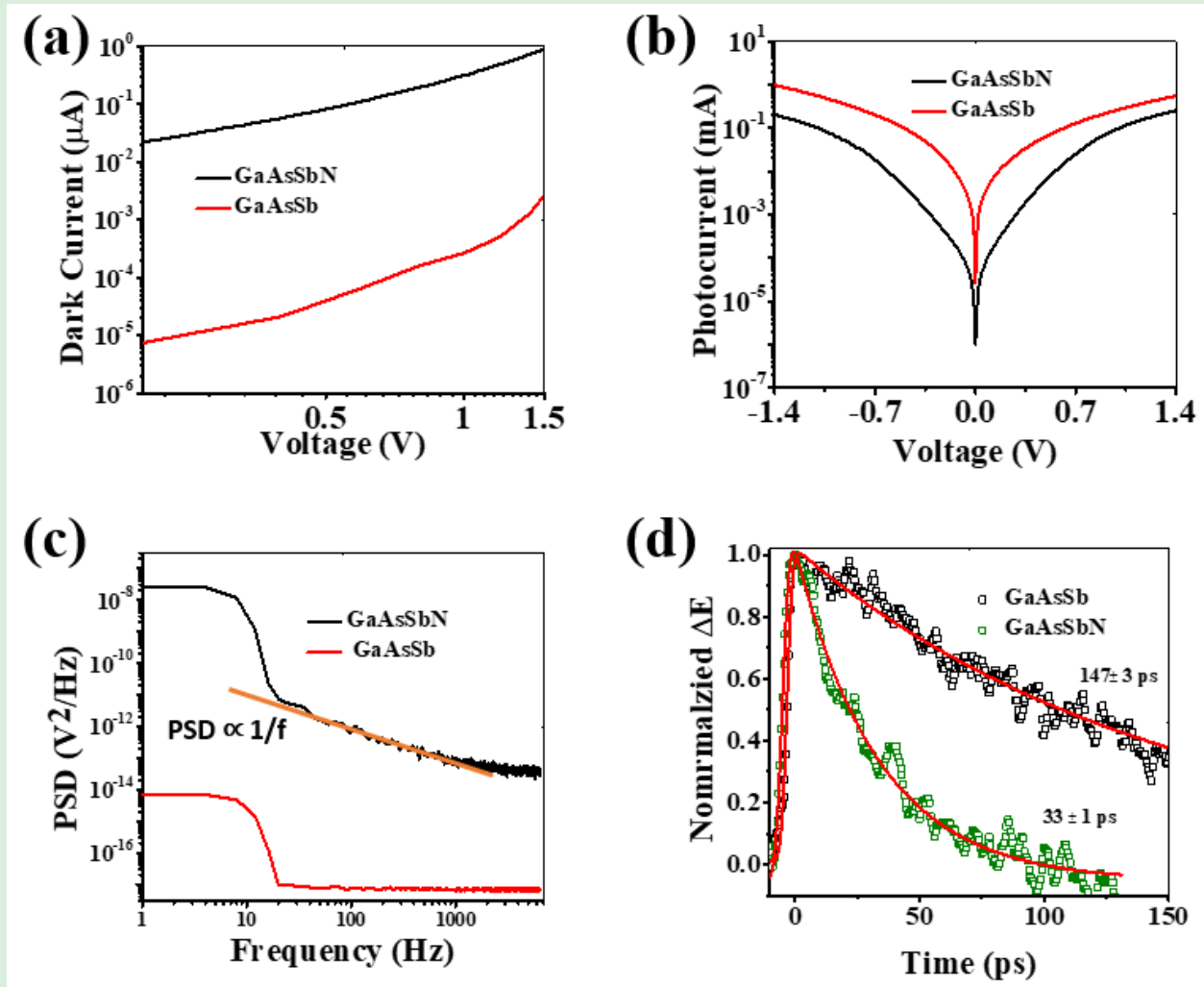


Figure 3. Electrical characterization of GaAsSb and GaAsSbN NW devices. Superimposed (a) dark current in a log-log scale. (b) photocurrent on a semilog scale. (c) low-frequency noise (LFN) data and $1/f$ trend line fit to the GaAsSbN data under dark conditions, and (d) transient photoinduced change in the THz electric (E) field for GaAsSb and GaAsSbN NWs probed by OPTP spectroscopy. The solid lines represent a single exponential fit convoluted with a Gaussian function.

The electrical characteristics of these two types of NWs were assessed using room temperature (RT) ensemble current-voltage (I-V) characterization and LFN spectroscopy. The magnitude of the dark current increased by almost three orders of magnitude, with a concomitant ~six-fold photocurrent reduction, in dilute nitride NWs compared to their non-nitride counterpart at 1 V reverse bias, as depicted in Figures 3(a) and 3(b), respectively. **These results correlate well with our transient conductivity measurements (Figure 2), which show that nitrogen incorporation substantially enhances the photocarrier scattering rate (Table 1), leading to a reduction in the carrier mobility by one order of magnitude.**

This significant deterioration of carrier transport properties in GaAsSbN nanowires further reduces photocurrent generation. Similarly, N incorporation in the NWs resulted in a ~ 6 order of magnitude higher noise level, as depicted in Figure 3(c). Further, the dilute nitride sample reveals $1/f$ noise as the dominant noise source for frequencies exceeding 15 Hz (as shown by the orange line representing a $1/f$ fit to our data in Fig. 3(c)), instead of the constant noise floor in GaAsSb NWs. For frequencies below 15 Hz, both devices exhibit generation-recombination (G-R) noise. This observed difference between the two samples above 15 Hz is attributed to the presence of N-induced defect states [21, 25, 52], which cause large potential fluctuations that are responsible for distributed relaxation time constants, broadening the G-R noise spectra, and causing $1/f$ noise to be the primary source of noise for higher frequencies.

Furthermore, the N-induced defects in the NW crystal lattice act as trap centers that enhance carrier relaxation [5], leading to a high dark current. The carrier recombination lifetimes in GaAsSbN and GaAsSb NWs, determined from ultrafast OPTP measurements (Figure 3(d)) by single-exponential fits to the carrier recombination dynamics, were extracted to be 33 ± 1 picoseconds (ps) and 147 ± 3 ps, respectively. Thus, the reduction in photocarrier lifetime with N incorporation (Fig. 3(b)) explains its adverse impact on the photocurrent. We note that this is especially noteworthy since the diameter of the GaAsSbN NWs is almost 50% larger than that of the GaAsSb NWs, which should result in longer carrier lifetimes since the lifetime is linearly proportional to NW diameter (section S2 in the supplementary information) [53]. This further underlines the role of N-induced defects in carrier relaxation.

In the literature, there are several reports of photocarrier lifetime measurements in GaAs [35, 54], InAs [35, 55], InP [35, 56], GaAsSb [57], GaInNAs [58], and GaPAsN [59] using OPTP. The photocarrier lifetime ranges from 1-5 ps in GaAs to 200-660 ps in InAs to ~ 1.4 ns in InP NWs [35]. Transient Rayleigh scattering (TRS) employed to study GaAsSb/InP heterostructured NWs revealed that NW core passivation led to a significant increase in photocarrier lifetime, from 10 ps in un-passivated NWs to 1800 ps in passivated NWs [57]. On the other hand, the carrier lifetime for a dilute nitride alloy in the thin film configuration is significantly reduced due to the incorporation of N-induced defects. A carrier lifetime of 2.6 ps was obtained using OPTP on a GaInNAs alloy thin film with 3% N incorporation [58]. Similarly, a

carrier lifetime of 23 ps was reported in GaPAsN (N=1.2%) thin films using optical transient absorption spectroscopy [59]. Therefore, the carrier lifetime of our dilute nitride NWs is better than those reported in dilute nitride thin films, indicative of their high quality.

In addition to excellent photocurrent generation, which is necessary to achieve a good photoresponse, a fast response time is strongly desirable for high-speed photodetection. Some insight into the high-speed properties of GaAsSb NWs is provided from our transient photoconductivity measurements. By fitting the carrier dynamics in Figure 3(d) with a sum of exponentials convoluted with a Gaussian function, rise times of 1.8 ± 0.1 ps and 2.2 ± 0.1 ps were obtained for our GaAsSb and GaAsSbN NWs, respectively. These rise time values are less than the 6 ps and 5 ps rise times measured previously in Au-catalyzed bare and passivated GaAs NWs, respectively [60]. However, one must be cautious in drawing any definitive conclusions, as the diameters of our GaAsSb NWs are significantly larger than the previously measured GaAs NWs, and they were also grown on different substrates. Nevertheless, the picosecond temporal response combined with picoampere dark currents suggests the strong potential of GaAsSb NWs for highly sensitive and ultrafast photodetection at telecom wavelengths.

4. Conclusion

In summary, our study of ultrafast carrier transport and recombination dynamics in Te-doped GaAsSb and Te-doped GaAsSbN NWs using OPTP spectroscopy directly reveals the impact of N incorporation on the quality of NWs and has been successfully correlated with the corresponding dark I-V and photoresponse characteristics. N-incorporation significantly reduces the carrier mobility and lifetime, causing significant deterioration in the PL, dark I-V, and photoresponse characteristics. A reduction in the bulk electron mobility from $1.64 \times 10^4 \text{ cm}^2\text{V}^{-1}\text{s}^{-1}$ to $1.48 \times 10^3 \text{ cm}^2\text{V}^{-1}\text{s}^{-1}$ and carrier recombination lifetime from 147 ± 3 ps to 33 ± 1 ps was observed upon $\leq 1\%$ N-incorporation in the Te-doped GaAsSb NWs. Our work offers a promising pathway for tailoring the carrier lifetime by defect engineering of this material system via controlled N incorporation. This will directly impact, for instance, the realization of NW-based optoelectronics photodetector devices with optimized speeds.

Acknowledgments

#L. Yuan and R. Pokharel contributed equally to this work. This work was performed, in part, at the Center for Integrated Nanotechnologies, an Office of Science User Facility operated by the U.S. Department of Energy (DOE) Office of Science. L.Y. and R.P.P. acknowledge support from the LANL LDRD Program. Los Alamos National Laboratory, an affirmative action-equal opportunity employer, is managed by Triad National Security, LLC for the U.S. Department of Energy's NNSA, under contract no. 89233218CNA000001. A portion of this work is supported through the U.S. Army Grant Number W911NF-19-1-0002 under the DoD HBCU/MI program and monitored by the Air Force Office of Scientific Research. It was also partly funded by the National Science Foundation (NSF) (Grant: EECS-18322117). Part of this work was performed at the Joint School of Nanoscience and Nanoengineering (JSNN), a member of the Southeastern Nanotechnology Infrastructure Corridor (SENIC) and the National Nanotechnology Coordinated Infrastructure (NNCI), which is supported by the NSF (Grant: ECCS-1542174).

References

1. Colace, L. and G. Assanto, *Germanium on Silicon for Near-Infrared Light Sensing*. IEEE Photonics Journal, 2009. **1**(2): p. 69-79.
2. Fu, T., et al., *A Si-based InP/InGaAs nanowire array photodetector operating at telecommunication wavelength*. Photonics and Nanostructures - Fundamentals and Applications, 2020. **40**: p. 100794.
3. Augel, L., et al., *Integrated Collinear Refractive Index Sensor with Ge PIN Photodiodes*. ACS Photonics, 2018. **5**(11): p. 4586-4593.
4. Li, X., et al., *The development of InGaAs short wavelength infrared focal plane arrays with high performance*. Infrared Physics and Technology, 2017. **80**: p. 112-119.
5. LaPierre, R.R., et al., *A review of III-V nanowire infrared photodetectors and sensors*. Journal of Physics D: Applied Physics, 2017. **50**(12): p. 123001.
6. Bulgarini, G., et al., *Nanowire Waveguides Launching Single Photons in a Gaussian Mode for Ideal Fiber Coupling*. Nano Letters, 2014. **14**(7): p. 4102-4106.
7. Ahmad, E., et al., *A Two-Step Growth Pathway for High Sb Incorporation in GaAsSb Nanowires in the Telecommunication Wavelength Range*. Scientific Reports, 2017. **7**(1): p. 10111.
8. Huh, J., et al., *Low frequency noise in single GaAsSb nanowires with self-induced compositional gradients*. Nanotechnology, 2016. **27**(38): p. 385703.
9. Anabestani, H., et al., *Review on GaAsSb nanowire potentials for future 1D heterostructures: Properties and applications*. Materials Today Communications, 2021. **28**: p. 102542.
10. Tossoun, B., et al., *High-Speed InP-Based p-i-n Photodiodes With InGaAs/GaAsSb Type-II Quantum Wells*. IEEE Photonics Technology Letters, 2018. **30**(4): p. 399-402.
11. Ungaro, G., et al., *GaAsSbN: a material for 1.3-1.55 μm emission*. Conference Proceedings. 2000 International Conference on Indium Phosphide and Related Materials (Cat. No.00CH37107), 2000: p. 553-556.
12. Hai, P., et al., *Direct determination of electron effective mass in GaNAs/GaAs quantum wells*. Applied Physics Letters, 2000. **77**(12): p. 1843-1845.

13. Tomić, S., et al., *Influence of conduction-band nonparabolicity on electron confinement and effective mass in GaN_xAs_{1-x}/GaAs quantum wells*. Physical Review B, 2004. **69**(24): p. 245305.
14. Erol, A., et al., *Dilute III-V nitride semiconductors and material systems*. Physics and Technology, 2008.
15. Li, J., et al., *Annealing effects on the temperature dependence of photoluminescence characteristics of GaAsSbN single-quantum wells*. Journal of Applied Physics, 2005. **98**(1): p. 013703.
16. Nunna, K., et al., *Optical studies of molecular beam epitaxy grown GaAsSbN/GaAs single quantum well structures*. Journal of Vacuum Science and Technology B: Microelectronics and Nanometer Structures Processing, Measurement, and Phenomena, 2007. **25**(3): p. 1113-1116.
17. Harmand, J., et al., *GaNAsSb: How does it compare with other dilute III-V-nitride alloys?*. Semiconductor Science and Technology, 2002. **17**(8): p. 778.
18. Harris Jr, J., et al., *MBE Growth and Characterization of Long Wavelength Dilute Nitride III-V Alloys*. Dilute Nitride Semiconductors, 2004: p. 1-92.
19. Bharatan, S., et al., *The effects of annealing on the structural, optical, and vibrational properties of lattice-matched GaAsSbN/GaAs grown by molecular beam epitaxy*. Journal of Applied Physics, 2007. **102**(2): p. 023503.
20. Iyer, S., et al., *Effects of N incorporation on the structural and photoluminescence characteristics of GaSbN/GaSb single quantum wells*. Journal of Applied Physics, 2007. **101**(11): p. 113508.
21. Sharma, M., et al., *Growth of defect-free GaAsSbN axial nanowires via self-catalyzed molecular beam epitaxy*. Semiconductor Science and Technology, 2017. **32**(12): p. 125003.
22. Kasanaboina, P.K., et al., *Self-catalyzed growth of dilute nitride GaAs/GaAsSbN/GaAs core-shell nanowires by molecular beam epitaxy*. Applied Physics Letters, 2015. **107**(10): p. 103111.
23. Chen, S., et al., *Dilute nitride nanowire lasers based on a GaAs/GaNAs core/shell structure*. Nano Letters, 2017. **17**(3): p. 1775-1781.
24. Sukritanon, S., et al., *Growth and characterization of dilute nitride GaN_xP_{1-x} nanowires and GaN_xP_{1-x}/GaN_yP_{1-y} core/shell nanowires on Si (111) by gas source molecular beam epitaxy*. Applied Physics Letters, 2014. **105**(7): p. 072107.
25. Deshmukh, P., et al., *Molecular beam epitaxial growth of GaAsSb/GaAsSbN/GaAlAs core-multishell nanowires for near-infrared applications*. Nanotechnology, 2019. **30**(27): p. 275203.
26. Johnson, S., et al., *Study of patterned GaAsSbN nanowires using sigmoidal model*. Scientific Reports, 2021. **11**(1): p. 1-14.
27. Buyanova, I. and W. Chen, *Physics and applications of dilute nitrides*. 2004: CRC Press.
28. Ahmad, E., et al., *Te incorporation in GaAs_{1-x}Sb_x nanowires and p-i-n axial structure*. Semiconductor Science and Technology, 2016. **31**(12): p. 125001.
29. Devkota, S., et al., *A study of n-doping in self-catalyzed GaAsSb nanowires using GaTe dopant source and ensemble nanowire near-infrared photodetector*. Nanotechnology, 2020. **31**(50): p. 505203.
30. Pokharel, R., et al., *Epitaxial high-yield intrinsic and Te-doped dilute nitride GaAsSbN nanowire heterostructure and ensemble photodetector application*. ACS Applied Electronic Materials, 2020. **2**(9): p. 2730-2738.
31. Ramaswamy, P., et al., *A study of dopant incorporation in Te-doped GaAsSb nanowires using a combination of XPS/UPS, and C-AFM/SKPM*. Scientific Reports, 2021. **11**(1): p. 8329.
32. Nalamati, S., et al., *Hybrid GaAsSb/GaAs Heterostructure Core-Shell Nanowire/Graphene and Photodetector Applications*. ACS Applied Electronic Materials, 2020. **2**(10): p. 3109-3120.
33. Sharma, M., et al., *Improved performance of GaAsSb/AlGaAs nanowire ensemble Schottky barrier based photodetector via in situ annealing*. Nanotechnology, 2018. **30**(3): p. 034005.
34. Nalamati, S., et al., *A Study of GaAs_{1-x}Sb_x Axial Nanowires Grown on Monolayer Graphene by Ga-Assisted Molecular Beam Epitaxy for Flexible Near-Infrared Photodetectors*. ACS Applied Nano Materials, 2019. **2**(7): p. 4528-4537.

35. Joyce, H.J., et al., *Electronic properties of GaAs, InAs and InP nanowires studied by terahertz spectroscopy*. Nanotechnology, 2013. **24**(21): p. 214006.
36. Boland, J.L., et al., *Modulation doping of GaAs/AlGaAs core-shell nanowires with effective defect passivation and high electron mobility*. Nano Letters, 2015. **15**(2): p. 1336-1342.
37. Liu, H., et al., *Ultra-high photoconductivity of bandgap-graded CdSxSe1-x nanowires probed by terahertz spectroscopy*. Scientific Reports, 2016. **6**(1): p. 1-7.
38. Joyce, H.J., et al., *The influence of surfaces on the transient terahertz conductivity and electron mobility of GaAs nanowires*. Journal of Physics D: Applied Physics, 2017. **50**(22): p. 224001.
39. Boland, J.L., et al., *High electron mobility and insights into temperature-dependent scattering mechanisms in InAsSb nanowires*. Nano Letters, 2018. **18**(6): p. 3703-3710.
40. Qian, Y., et al., *Rapid, facile synthesis of InSb twinning superlattice nanowires with a high-frequency photoconductivity response*. RSC Advances, 2021. **11**(32): p. 19426-19432.
41. Beaudoin, A., et al. *Carrier dynamics in silicon nanowires studied using optical-pump terahertz-probe spectroscopy*. In APS March Meeting Abstracts, 2014.
42. Bae, J.M., et al., *Ultrafast photocarrier dynamics related to defect states of Si 1-x Ge x nanowires measured by optical pump-THz probe spectroscopy*. Nanoscale, 2017. **9**(23): p. 8015-8023.
43. Fotev, I., et al. *Pump-probe THz spectroscopy study of electronic properties of semiconductor nanowires*. 44th International Conference on Infrared, Millimeter, and Terahertz Waves (IRMMW-THz), IEEE, 2019.
44. 박담비, et al., *Ultrafast carrier dynamics of the topological insulator Bi₂Te₃ nanowire with the first and second surface states*. 56th Winter Technical Conference, Korean Society of Vacuum Engineers, 2019. p. 40-40.
45. Parkinson, P., et al., *Noncontact measurement of charge carrier lifetime and mobility in GaN nanowires*. Nano Letters, 2012. **12**(9): p. 4600-4604.
46. Joyce, H.J., et al., *A review of the electrical properties of semiconductor nanowires: insights gained from terahertz conductivity spectroscopy*. Semiconductor Science and Technology, 2016. **31**(10): p. 103003.
47. Nunna, K., et al., *Nitrogen incorporation and optical studies of Ga As Sb N / Ga As single quantum well heterostructures*. Journal of Applied Physics, 2007. **102**(5): p. 053106.
48. Tang, H., et al., *Carrier dynamics in Si nanowires fabricated by metal-assisted chemical etching*. ACS Nano, 2012. **6**(9): p. 7814-7819.
49. Parkinson, P., et al., *Transient Terahertz Conductivity of GaAs Nanowires*. Nano Letters, 2007. **7**(7): p. 2162-2165.
50. Boland, J.L., et al., *Increased Photoconductivity Lifetime in GaAs Nanowires by Controlled n-Type and p-Type Doping*. ACS Nano, 2016. **10**(4): p. 4219-4227.
51. Balaghi, L., et al., *High electron mobility in strained GaAs nanowires*. Nature Communications, 2021. **12**(1): p. 1-11.
52. Kasanaboina, P., et al., *Effects of annealing on GaAs/GaAsSbN/GaAs core-multi-shell nanowires*. Nanoscale Research Letters, 2016. **11**(1): p. 1-6.
53. Grumstrup, E.M., et al., *Ultrafast carrier dynamics in individual silicon nanowires: characterization of diameter-dependent carrier lifetime and surface recombination with pump-probe microscopy*. The Journal of Physical Chemistry C, 2014. **118**(16): p. 8634-8640.
54. Afalla, J., et al. *Photo-carrier dynamics of MBE-grown GaAs on silicon studied by optical-pump terahertz-probe*. 43rd International Conference on Infrared, Millimeter, and Terahertz Waves (IRMMW-THz), IEEE, 2018.
55. Beleckaitė, I., L. Burakauskas, and R.J.L.J.o.P. Adomavičius, *Study of surface electric field and photocarrier dynamics in InAs by means of a modified double-pump-pulse terahertz emission method*. Lithuanian Journal of Physics, 2018. **58**(1).
56. Chen, Y., et al., *Optimization of the short-circuit current in an InP nanowire array solar cell through opto-electronic modeling*. Nanotechnology, 2016. **27**(43): p. 435404.

57. Shojaei, I.A., et al., *Strong hot carrier effects in single nanowire heterostructures*. Nano Letters, 2019. **19**(8): p. 5062-5069.
58. Mangeney, J., et al., *Picosecond carrier lifetimes in dilute GaInNAs grown on InP substrate*. Applied Physics Letters, 2011. **99**(14): p. 141902.
59. Heyman, J., et al., *Carrier Lifetimes in a III–V–N Intermediate-Band Semiconductor*. Physical Review Applied, 2017. **7**(1): p. 014016.
60. Gallo, E.M., et al., *Picosecond response times in GaAs/AlGaAs core/shell nanowire-based photodetectors*. Applied Physics Letters, 2011. **98**(24): p. 241113.